Published in final edited form as:
Biochemistry. 2010 November 9; 49(44): 9667–9676. doi:10.1021/bi101261x.

Zinc binding drives sheet formation by the SAM domain of diacylglycerol kinase δ

Mary Jane Knight[1], **Marisa K. Joubert**[2], **Megan L. Plotkowski**[1], **Janette Kropat**[1], **Mari Gingery**[1], **Fumio Sakane**[3], **Sabeeha S. Merchant**[1], and **James U. Bowie**[*]

[1] Department of Chemistry and Biochemistry, Institute of Genomics and Proteomics and the Molecular Biology Institute, University of California, Los Angeles, Los Angeles, California 90095-1570

[2] Amgen Inc., Thousand Oaks, CA 91320

[3] Department of Chemistry, Graduate School of Science, Chiba University, Chiba, Japan

Abstract

The Diacylglycerol Kinase (DGK) family of enzymes plays critical roles in lipid signaling pathways by converting diacylglycerol to phosphatidic acid, thereby downregulating signaling by the former and upregulating signaling by the latter second messenger. Ten DGK family isozymes have been identified to date, which possess different interaction motifs imparting distinct temporal and spatial control of DGK activity to each isozyme. Two DGK family members, δ and η, contain a Sterile Alpha Motif (SAM) domain. The SAM domain of DGKδ1 forms helical polymers that are important for retaining the enzyme in cytoplasmic puncta, thereby inhibiting activity at the plasma membrane until pathway activation. Because zinc was found to be important for stabilizing the similar SAM polymers of the scaffolding protein Shank-3, we investigated the potential role of zinc in DGKδ SAM domain (DGKδSAM) assembly. We find that DGKδSAM binds zinc at multiple sites, driving the organization of the DGKδSAM into large sheets of polymers. Moreover, a mutant DGKδ containing a SAM domain refractory to zinc binding diminishes the formation of cytoplasmic puncta, shows partially impaired regulation of transport to the plasma membrane, and lacks the ability to inhibit the formation of CopII coated vesicles. These results suggest that zinc may play an important role in the assembly and physiology of the DGKδ isozyme.

Keywords

Sterile Alpha Motif; polymer; CopII

Diacylglycerol (DG) serves as an intermediate in lipid metabolism and also acts as a powerful second messenger known to influence cell proliferation and differentiation, at least in part through the allosteric activation of protein kinase C (1). The primary means of downregulating DG in the cell is through DGK-catalyzed formation of phosphatidic acid (PA). PA also serves as a second messenger lipid in signaling pathways that involve metabolic and mitogenic cell responses (2). Both DG and PA levels must, therefore, be tightly regulated. Highly specific spatial and temporal control of DGK activity in different cell types is achieved in part by the presence of diverse regulatory domains attached to the

[*]Direct correspondence to: James U. Bowie, Ph.D., 611 Charles E. Young Drive, 655 Boyer Hall, Los Angeles, CA 90095. Phone: 310-206-4747 Fax: 310-206-4749 bowie@mbi.ucla.edu.

SUPPORTING INFORMATION
Supporting figures S1-4. This material is available free of charge via the Internet at http://pubs.acs.org.

common catalytic core (3). Based on their domain structures, the DGK enzymes can be grouped into five subfamilies (3). DGK enzymes of the type II DGK subfamily (δ, η, κ) are characterized by an N-terminal Plekstrin Homology (PH) domain and catalytic and accessory domains (4.-6). The closely related δ and η members also contain a C-terminal SAM domain (4.,7).

Two splice variants of DGKδ, DGKδ1 and DGKδ2, have been identified with divergent cellular distributions and response to stimuli. DGKδ2 is identical to DGKδ1 except for the addition of 52 residues at the N terminus. Both DGKδ1 and δ2 splice variants can be found in a punctate, cytoplasmic distribution in the absence of cell stimulation (8.,9). A fraction of the DGKδ2 puncta colocalize with markers for Clathrin-coated vesicles and DGKδ2 kinase activity is required for efficient uptake of cell surface receptor cargo into these vesicles (10). The nature of the puncta formed by the δ1 isoform is unknown, but DGK δ1 has also been shown to associate with the endoplasmic reticulum membrane and inhibit anterograde ER-to-Golgi transport when overexpressed (11). DGKδ1 relocalizes to the plasma membrane upon stimulation with 12-O-tetradecanoylphorbol-13-acetate (TPA) (8). DGKδ1 deficiency has also been implicated in the development of hyperglycemia-induced insulin resistance and thus may contribute to the progression of Type II diabetes (12).

The DGKδSAM domain, which is found in both splice variants, is required for association of DGKδ1 with the ER (11), inhibition of CopII coated vesicle formation (10), and for retention of DGKδ1 in its punctate, cytoplasmic distribution in the absence of stimulation (11). DGKδSAM forms polymers with features that are quite similar to polymers formed by other SAM domains (13.-16). In particular, our earlier crystal structure of DGKδSAM revealed a left-handed helical polymer with six subunits per turn shown in Figure 1 (17). The subunits within the polymer associate via two distinct surfaces on the SAM domain called the Mid-Loop (ML) surface and the End-Helix (EH) surface (13). Mutations in the polymer interface that reduce subunit association affinity lead to a redistribution of DGKδ from the cytoplasmic puncta to the plasma membrane (8), suggesting that polymerization is important for maintenance of the protein in the cytoplasm.

A closely related SAM domain from the rat Shank-3 protein (Shank3SAM) also forms polymers, but these polymers can associate in a side-by-side fashion to create sheets (14). The sheets become highly ordered in the presence of zinc ions. We therefore hypothesized that zinc might also serve to organize DGK into a higher-order assembly and might have an impact on enzyme localization and function. Here we show that DGKδ-SAM does indeed bind zinc, leading to sheet formation that may be important for its biological function.

Experimental Procedures

Cloning

DGKδ1-WT (residues 1097–1163 of the full-length protein which corresponds to residues 1–66 of the SAM domain) was inserted into the pMALc2x vector (Novagen) using SalI and HindIII sites to generate MBP-DGKδSAM-WT. Mutations and deletions were introduced into all constructs using Quickchange mutagenesis (Stratagene) and confirmed by sequencing (Genewiz).

For the DGKδSAM-V52E and DGKδSAM-E35G constructs that were used in tag-free applications, the DGKδSAM domain (containing the residues specified above) was PCR amplified and ligated into a modified pET3c vector that contains the expression leader sequence MEKTR followed by a His_6 tag and a tobacco etch virus (TEV) protease site, ENLYFQG, N-terminal to the DGKδSAM sequence such that the His_6 tag could be

removed. The E35G and V52E mutations were introduced as described above. After cleavage the DGKδSAM-V52E protein contains an added N-terminal G and C-terminal RD.

pEGFP-DGKδ-WT (GFP-DGKδ1-WT) and pEGFP-DGKδ1(V52E) (GFP-DGKδ1-V52E) constructs were described previously (17). The GFP-DGKδ1-ΔSAM was generated by deleting residues 1097–1163 via Quickchange mutagenesis using primers with complementary sequences to the immediately upstream and downstream portions of the DGKδ construct.

Protein Purification

All MBP fusion constructs were expressed in ARI814 cells. The cells were grown at 37°C in LB media supplemented with 100 μg/ml Ampicillin until the cell density reached an OD_{600} of 0.8. Protein expression was induced with 1 mM isopropyl-β-D-galactopyranoside (IPTG) and incubated at 37°C for an additional two hours at which point the cells were harvested by centrifugation. 40 g of cell pellet was resuspended in 140 mL of 20 mM Tris (pH 7.5), 200 mM NaCl, 1 mMTCEP, 5 mM $MgCl_2$ containing lysozyme (1 mg/mL), DnaseI (10 ug/mL), 0.5 mM PMSF, and eight tablets of Complete Protease Inhibitor (Roche). The cells were lysed by sonication and the lysate was centrifuged at 27,000 × g for 45 minutes. The supernatant was incubated with 50 mL Amylose resin (New England Biolabs) for one hour at 4°C. The resin was poured into a column and washed with seven column volumes of 20 mM Tris (pH 7.5), 300 mM NaCl, 1 mM TCEP and protein was eluted in 20 mM Tris (pH7.5), 200 mM NaCl, 1 mM TCEP, with 10 mM maltose. In order to separate proteolyzed, free MBP from the intact fusion protein, the eluted protein was then applied to a 5 mL IMAC-HP column (GE Biosciences) charged with zinc acetate and the bound protein was eluted in 15 mL of 20 mM Tris (pH 7.5), 200 mM NaCl, 1 mM TCEP, with 500 mM imidazole. MBP-DGKδSAM^{ZnMut} did not bind the zinc column but displayed essentially no proteolysis so this further purification step was not necessary. The protein was dialyzed at 4°C for four hours against 2 L of 20 mM Tris (pH 7.5), 200 mM NaCl, 1 mM TCEP and transferred to 2 L of the same buffer for overnight dialysis. Dialyzed protein was concentrated using an Amicon Ultra centrifugal filter concentrator unit (Millipore).

The DGKδSAM-V52E construct was transformed into BL21(DE3) cells and grown at 37°C in LB media supplemented with 100 μg/ml ampicillin until the cell density reached an OD_{600} of 0.6. Cells were induced with 1 mM IPTG and incubated at 37°C for an additional five hours at which point they were harvested by centrifugation. 40 g of cell pellet was resuspended in 140 mL of 20 mM Tris (pH 7.5), 300 mM NaCl, 5 mM $MgCl_2$, 1 mMTCEP, containing 0.5 mM PMSF, lysozyme (1 mg/mL), and DnaseI (10 ug/mL). Cells were lysed as described above. Cell supernatant was applied to 3mL of Ni-NTA Superflow resin (Qiagen) and incubated for one hour. Resin was washed with 200 mL of the same buffer and eluted with buffer containing 300 mM Imidazole. The His_6 tag was cleaved with TEV protease S219V at 0.5 mg/ml DGK-SAM TEV at a mole ratio of 5:1 TEV to DGKδSAM and the reaction was incubated with mixing for 24 h at 4°. The cleaved mixture underwent two rounds of subtractive Ni-NTA affinity chromatography to remove the His tag, protease and uncleaved substrate. Cleaved protein was dialyzed and concentrated as described above.

Turbidity Assay

200 μl of 38 μM tag-free DGKδSAM-E35G protein in 20mM Tris (pH 7.5), 50mM NaCl was either incubated with 38 μM zinc acetate, 1mM EDTA, or a sequential combination of the two with a 20 min incubation between additions. After 24 hours at 4°C, samples were transferred to a UV/Vis transparent 96 well-microtiter plate and A_{350} was measured using a SpectraMax Plus microplate reader (Molecular Devices). Samples were prepared in triplicate and the average calculated. In order to construct a turbidity curve for increasing

concentrations of zinc acetate, 150 μl samples of 20 μM tag-free DGKδSAM-E35G were individually incubated with 5 μl of a dilution series of zinc acetate such that the range of final zinc concentrations spanned from 0 to 57 μM. After 24 h incubation at 4°C, samples were assayed as above.

Gel Filtration

500 μL of 16.5 μM MBP-DGKδSAM-WT, MBP-DGKδSAM^{ZnMut}, and MBP protein in 20mM Tris (pH 7.5), 500 mM NaCl was incubated with 1mM EDTA for 30 minutes at room temperature. Protein solutions were then centrifuged for 10 minutes at 16,000 × g. Protein was loaded onto a Superdex200-10/300GL gel filtration column (Amersham Biosciences) at 0.5 mL/min.

Zinquin Fluorescence Assay

200 μL samples of 37 μM tag-free DGKδSAM-WT protein in 20mM Tris pH 7.5/50 mM NaCl were independently incubated with either 7.4 μM zinc acetate or zinc-free buffer for 30 min at room temperature and samples were centrifuged to separate the precipitated fraction. Samples were prepared in triplicate. Supernatant was transferred to a separate tube and precipitate was washed with three successive 500 μL washes of zinc-free buffer. The precipitated protein was then resolublized in 200 μL 8 M Urea. The final urea concentration of all samples (supernatant, precipitated protein fractions, and protein incubated in zinc-free buffer) was adjusted to 6 M urea in 20 mM Tris (pH 7.5), 50mM NaCl. 200 μL of each sample was then incubated with 50 μM Zinquin ethyl ester and incubated at room temperature for 30 min. Zinquin fluorescence was monitored in 96-well clear bottom, black sided plates (Nunc) on a Molecular Devices Spectramax M5 plate reader using an excitation wavelength of 368 nm, an emission wavelength of 510 nm, and a cutoff filter of 495 nm. Protein concentration was measured by absorbance at 280 nm on a Nanodrop spectrophotometer (Thermo Scientific).

Electron Microscopy

Protein samples in 5 mM Tris (pH 7.5), 50 mM NaCl, and 6 M urea were dialyzed into the same buffer without urea either with or without 1mM zinc acetate. Carbon-coated parlodion support films mounted on copper grids were made hydrophilic immediately before use. Approximately 3 μL of each protein sample was applied to separate grids and allowed to adhere for several minutes. Grids were rinsed with distilled water and negatively stained with 1% uranyl acetate. Samples were examined in a Hitachi H-7000 electron microscope at an accelerating voltage of 75kV.

ICP-MS Analysis of Purified MBP-DGKδSAM Mutant

5 mL each of 16 μM MBP-DGKδSAM constructs and MBP were dialyzed into 2L of 20mM Tris pH 7.5, 50 mM NaCl, 1 mM zinc acetate for 24 hours and then transferred to 2 L fresh buffer for an additional 24 hours. In the case of the metal competition assay, MBP and MBP-DGKδSAM-WT were dialyzed into 20mM Tris pH 7.5, 50 mM NaCl, 160 μM zinc sulfate, 160 μM cobalt sulfate, 160 μM copper sulfate, 160 μM manganese sulfate and 160 μM magnesium sulfate as above. After metal incubation was complete, samples were dialyzed against 4 L of 20mM Tris pH 7.5, 50 mM NaCl for 10 hours followed by three successive transfers into fresh buffer. Samples were transferred to acid-washed 15 mL conical tubes and ultra pure nitric acid was added to a final concentration of 5%. Samples were incubated at 60°C until no particulate matter could be observed. Ultra pure water was added to adjust the final nitric acid concentration to 2.4%. Yttrium and Gallium were added as internal standards to all samples and a serial dilution of standard CL-CAL-2 (Claritas) was used to create a standard curve for all metals measured. Samples were analyzed using

an Agilent 7500ce Quadrupole ICP-MS. One isotope for each metal (Mg 24, Mn 55, Co 59, Ni 60, Cu 63, and Zn 66) was measured and total metal occupancy was extrapolated.

Surface Plasmon Resonance

The surface plasmon resonance experiments were performed at 20°C on a Biacore T100 instrument, essentially as described previously (17). Either MBP-DGKSAM-V52E or MBP-DGKSAM-H38A/V52E was immobilized on a Biacore CM5 sensor chip via EDC/NHS crosslinking and various concentrations of MBP-DGKSAM-E35G were applied to the chip in 0.01 M HEPES (pH 7.4), 0.15 M NaCl, 3 mM EDTA, 0.005% surfactant P20 until equilibrium binding was achieved. The resulting binding data were fit to a 1 to 1 binding model using Kaleidagraph software.

Cell Culture and Transfection

Human embryonic kidney (HEK293) cells and Cos-7 cells stably expressing Sec13-YFP were maintained at 37°C in High Glucose DMEM (Gibco) supplemented with 10% fetal bovine serum (FBS). To prepare cells for transfection, they were grown on chamber slides (Nunc) for one day. Transfections and co-transfections of plasmids (pEGFP-DGKδ1-WT, pEGFP-DGKδ1-V52E, pEGFP-DGKδ1$^{\Delta SAM}$, pEGFP-DGKδ1^{ZnMut}, and mCherry-Clathrin) were carried out using Lipofectamine or Lipofectamine LTX (Invitrogen) per the manufacturer's instructions. The media was replaced with DMEM supplemented with 10% FBS and cells were incubated for an additional two days before use.

TPA Induction

Cells transfected with either pEGFP-DGKδ1^{WT} or pEGFP-DGKδ1^{ZnMut} were washed with PBS and media was replaced with DMEM containing 10% FBS and 0.1% BSA. After a three hour incubation, cells were exchanged into the same media containing 0.00, 0.15, 0.30, 0.45, 0.60, 0.75, 0.90, or 1.05μM TPA and incubated for one hour.

Confocal Microscopy

Cells were fixed onto slides for 10 minutes using 3.7% Formaldehyde in PBS, washed twice with PBS, and mounted using ProLong Gold Antifade Reagent with Dapi (Invitrogen). Cells were visualized using a Leica TCS-SP2 AOBS Confocal Microscope and images were processed using Leica Confocal Software. The estimated ratio of GFP fluorescence in the PM region versus the cytosolic region in the TPA-stimulated cells was determined by taking a line intensity profile through a given cell using the ImageJ software. The PM-region fluorescence was defined as the average fluorescence of the 1 μm segment that contains a fluorescence signal above background and the cytosolic-region fluorescence was defined as the average fluorescence of 1 μm, 0.5 μm to the interior of the cell from the defined PM region. A PM/cytosol fluorescence ratio was then calculated for each edge of the cell, two ratios per line profile. The averages from three lines drawn at different angles through the cell were then averaged to get an overall average ratio for a given cell. The average ratios from 20 cells of each sample were averaged to obtain overall population averages. A two-tailed T-test was performed in Microsoft Excel assuming heteroscedastic populations.

RESULTS

DGKδSAM Binds Zinc

To test whether DGKδSAM is capable of binding a metal ion with high affinity and specificity we performed a metal-retention competition assay. We dialyzed a DGKδSAM-WT-maltose binding protein (MBP) fusion (MBP-DGKδSAM-WT) into a buffer containing zinc, cobalt, copper, manganese, and magnesium, each in 10-fold molar excess for 46 hours.

The MBP fusion was utilized as a solubility-enhancing factor. The protein was then dialyzed extensively against metal-free buffer. MBP does not contain a metal binding site and was used as a negative control. Inductively coupled mass spectrometry (ICP-MS) analysis indicates that while MBP retains a negligible amount of any of the metal ions included in the experiment, MBP-DGKδSAM-WT retains considerable zinc and a small amount of copper (Fig. 2A). While the possibility that there is a copper-specific binding site in addition to one or more separate zinc-binding sites cannot be excluded, the similarity of copper and zinc metalloprotein binding sites (18.-22) and the inherently more stable copper-protein ligand interaction per the Irving-Williams series trend (23), combined with the fact that zinc is more abundant than copper in the human body (24) suggests that the retained copper may be the result of promiscuous binding by a zinc-specific site.

A zinc binding site that is self contained within a single protein subunit can yield a total maximum occupancy of 100% and a zinc binding site that is shared between two subunits can contribute a total maximum occupancy of 50%. The molar occupancy of zinc observed for the wild type protein was 116.6% despite extensive dialysis. This suggests that there is at least one high affinity zinc binding site and potentially additional binding sites, particularly if copper is occupying some fraction of the sites that normally accept zinc.

Zinc induces assembly into sheets

We observed that adding zinc to the MBP-DGKδSAM-WT construct caused a fraction of the protein to precipitate. This phenomenon allowed us to investigate whether zinc binding could drive the higher-order assembly of DGKδSAM, using a simple turbidity assay. DGKδSAM-E35G is a mutant of DGKδSAM that exhibits greatly reduced polymerization as position 35 lies buried in the subunit interface. As shown in Fig. 2B and C, when one molar equivalent of zinc acetate was added to a solution of 38 μM DGKδSAM-E35G, turbidity increased dramatically, indicating some degree of aggregation. In contrast, maltose binding protein (MBP), which does not bind zinc, showed no increase in turbidity upon zinc addition (not shown). The addition of EDTA to a sample after it reached maximal turbidity caused a reduction in turbidity to nearly the original level, indicating that the aggregation process is reversible. Samples which were incubated with EDTA followed by addition of zinc showed a negligible increase in turbidity. These results suggest that zinc binding may enhance the assembly of DGKδ-SAM. If the aggregates are formed by SAM polymers, zinc binding must be able to overcome the decrease in subunit binding affinity imparted by the E35G mutation.

If we assume that turbidity reflects zinc binding, we can obtain an upper estimate of the zinc dissociation constant (K_d). In particular, 20 μM DGKδSAM-E35G was incubated with 0 to 57 μM zinc acetate solution followed by turbidity measurement. The maximal turbidity response was attained at a zinc concentration of 20 μM zinc acetate suggesting stoichiometric zinc binding at this protein concentration (Fig. 2B). This indicates that the zinc K_d must be well below 10 μM.

If zinc causes DGKδSAM precipitation by stabilizing large oligomeric structures, zinc should preferentially associate with the insoluble fraction of the protein. Samples of DGKδSAM-E35G incubated with an excess of zinc are shifted entirely to the insoluble fraction so a limiting concentration of zinc was added to protein samples such that both soluble and insoluble fractions could be isolated. Both fractions were denatured and assayed with zinquin, a zinc-responsive fluorophore, to determine whether the protein populations retained zinc ions. The total normalized fluorescence of the samples per μmol of protein shown in Figure 2D. The zinc-precipitated fraction does indeed display more than three times as much zinquin fluorescence per μmol of protein than the protein in the soluble fraction. Without zinc supplementation, DGKδSAM-E35G also displays a measurable

zinquin signal suggesting that the purified protein retains some amount of zinc that became bound in the cell or during the course of purification, a further indication of a high affinity zinc binding site.

To investigate the nature of the zinc-induced aggregate, we examined it by electron microscopy (EM). Figure 3 shows negative stain EM images of DGKδSAM-E35G in the presence and absence of zinc. Gel filtration chromatography indicates that most of the DGKδSAM-E35G protein sample is monomeric in the absence of zinc (not shown), but in the EM field we found occasional polymers that show a propensity to associate side-by-side forming thin ribbons (Fig. 3A). It is possible that these polymer assemblies are assisted by the small amount of zinc retained during purification as described above. In the presence of added zinc, DGKδSAM-E35G organizes into large sheet structures (Fig. 3B and C). In the presence of 50 μM zinc acetate large, folded sheet structures are common and in 1 mM zinc acetate the grid is entirely covered in large layers of sheets with rare breaks in the continuous structure. A second monomeric mutant of DGKδSAM (DGKδSAM-V52E) was also examined by EM (Fig. S1). V52E is a stronger monomeric mutation in that a larger percentage of the protein population exists as monomers (17), reflected by the fact that no polymers are visible in zinc-free conditions. After zinc addition, however, large sheet structures visually identical to those seen in the DGKδSAM-E35G sample appear. While the sheets appear largely smooth and featureless, in both samples the sheet edges are straight and striations in the sheet structure can be seen in some of the darkly stained regions, supporting a model in which polymers associate longitudinally to form the massive sheets. These sheets thus appear to be quite similar to the sheets observed for Shank3SAM, which are also stabilized by zinc ions.

In the crystal structure of Shank3SAM, helical polymers associated side by side into parallel and antiparallel sheets, which were predicted to approximate the quaternary structure of the sheets visualized by EM (14). As shown in Fig. 4, similar packing is also present in the DGKδSAM-E35G structure (17). If the side-by-side packing elements represent the sheet structure, the DGKδSAM sheet interface is far more densely packed than the interface observed for Shank3SAM, due in part to the smaller helical pitch of the DGKδSAM polymer (Fig. 1). This higher packing density is consistent with the low level of detail observed in the micrographs of DGKδSAM sheet structures as the negative stain would be unable to penetrate deeply into the tightly packed crevasses between subunits and polymers.

Construction of a DGKδSAM mutant refractory to zinc

The results presented so far indicate that zinc binding can dramatically stabilize higher order oligomerization of DGKδSAM *in vitro*. In particular, the polymers observed previously can be packed side-by-side to create sheet structures. To investigate whether zinc induced sheet formation is important for the biological function of DGKδ a mutant of DGKδSAM was constructed that could still form polymers like the wild-type protein, but could no longer bind zinc and could therefore not form stable sheets.

To construct a zinc refractory mutant, it was necessary to identify residues involved in zinc binding. Attempts to identify the zinc binding residues by obtaining crystals of DGKδSAM in the presence of zinc were unsuccessful. Moreover, the zinc binding site found in Shank3SAM is not completely conserved in DGKδSAM, making it unlikely to bind zinc in an identical manner. (Fig. S2) To circumvent the lack of structural data, Hotpatch (25), a statistical prediction program capable of identifying potential metal-binding sites, was employed providing a list of residues that were most likely to be involved in zinc binding (His3, Cys20, Glu21, His38, Cys60). These residues clustered into two potential Zn sites. One cluster is within the polymer (intra-polymer) and involves residues His38 and Cys60 (Fig. 4A). A second cluster involves residues His3 and Cys20 and would be located between

polymers (inter-polymer), possibly stabilizing the side-by-side assembly of the polymers. As both parallel and anti-parallel arrangements of the polymers are seen in the crystal, there are two ways the inter-polymer residues could cluster as illustrated in Figure 4, B and D. After further examination of these potential sites, we added residues Glu8, Glu9, Glu15, His16, Lys23, Thr27, Ser34, Glu35, Lys56, and Lys63 to our list of potential zinc binding residues.

To test the importance of the selected residues in zinc binding, each residue was changed individually to alanine and the mutants were assessed for zinc binding. The mutant proteins were incubated in 1mM EDTA for 36 hours, then dialyzed into a solution of 1mM zinc acetate, and then dialyzed extensively against zinc-free buffer. Finally, the molar zinc occupancy of each mutant protein was determined by ICP-MS.

No single mutation eliminated zinc binding, consistent with the possibility of more than one zinc binding site. Nevertheless, of the 15 single mutants tested, five showed somewhat diminished Zn occupancy: H3A, H16A, C20A, H38A, C60A (Fig. 5A). C20A, located in a potential site between polymers, showed the largest drop in zinc occupancy. Notably, C20S appeared as a frequent mutation that rendered DGKδSAM soluble in a previous *in vivo* soluble mutant selection (17). To eliminate Zn binding, we therefore combined the single mutations that reduced occupancy. As shown in Fig. 5A, by combining H3A, C20A, H38A, C60A we were able to reduce zinc retention to 3%. We define the zinc binding deficient quadruple mutant as DGKδSAM^{ZnMut}.

As expected, the DGKδSAM^{ZnMut} construct does not show any increase in turbidity after incubation with 50 μM zinc acetate, further indicating the importance of zinc in sheet formation (not shown). Moreover, EM images of DGKδSAM^{ZnMut} showed a minimal effect of zinc on oligomerization (Fig. 3E). In the absence of zinc, short polymers are observed for DGKδSAM^{ZnMut}, much like the wild-type protein. When zinc is added to the DGKδSAM^{ZnMut}, however, polymers increase in prevalence and length marginally but no large sheet structures are formed in 50 μM zinc. Thus, the DGKδSAM^{ZnMut} appears to be largely refractory to the effects of zinc.

DGKδSAM^{ZnMut} can still form polymers in the absence of zinc

As shown in Figure 5B, MBP-DGKδSAM^{ZnMut} protein migrated through a gel filtration column at an elution volume similar to the wild type protein without zinc, consistent with an average molecular weight of 171 kD, or roughly 3.3 subunits. Thus, both the WT and DGKδSAM^{ZnMut} MBP fusion proteins at the same concentration form similar sized small oligomers in the absence of zinc, consistent with the EM results (above). The MBP fusion constructs form smaller oligomers compared to their tag-free counterparts most likely due to steric inhibition of continued polymer growth imparted by the bulky MBP protein.

Because H38A is near the polymer interface, we also tested the effect of this mutation on subunit affinity by surface plasmon resonance (SPR). We previously reported the K_d of the interaction at the wild type polymer interface to be 6.3 +/− 1.2 μM (17). We repeated these experiments in the presence of EDTA and found a slightly increased K_d of 12.2 +/− 2.3 μM (Fig. 6). In comparison, the K_d of an interface that includes the H38A mutation is 23.0 +/− 5.2 μM. Thus, the affinity of the polymer interface is only mimimally altered by the presence of the H38A mutation. We note that EDTA is insufficient to completely strip zinc from MBP-DGKδSAM constructs as shown in Figure 5A. Thus, the affinity we obtain for the interface must be evaluated with the caveat that the wild-type protein population will be contaminated with a small fraction of protein bound to zinc.

The DGKδSAM^{ZnMut} has altered enzyme localization

To assess the possible physiological role of DGKδSAM zinc binding, we tested DGKδSAM^{ZnMut} in the context of the full length protein in a series of cell biology assays. GFP-DGKδ1-WT and GFP-DGKδ1^{ZnMut} fusion constructs were transiently transfected into HEK293 cells. In the absence of TPA stimulation the mutant protein showed a decreased ability to localize to large cytoplasmic puncta. (Fig. 7A and B) As DGKδ2 protein has been previously shown to partially colocalize with clathrin (10), we transiently co-transfected GFP- DGKδ1-WT and mCherry-Clathrin but did not see a significant colocalization of the observed puncta, leaving the identity of DGKδ1 puncta in HEK293 cells unknown. (Fig. S3).

To test the effect of the DGKδSAM^{ZnMut} on signaling, we tested the response to TPA stimulation. TPA is a non-metabolizable DG analogue that has been previously shown to relocalize DGKδ1 protein to the plasma membrane(8). Populations of GFP-DGKδ1 transfected cells were stimulated with a TPA gradient from 0.15 to 1.05 μM. At low and intermediate TPA concentrations, the zinc binding deficient construct displayed a slightly increased propensity to relocalize to the plasma membrane relative to the wild type protein. At 0.45 μM TPA, most expressing the cells expressing the GFP-DGKδ1-WT construct have lost cytosolic puncta although a large percentage of the protein remains in the cytosol with an average PM-region to cytosolic-region fluorescence intensity ratio of 0.62 +/− 0.18. In comparison, a greater proportion of the GFP-DGKδ1^{ZnMut} protein appears to localize to the plasma membrane with a ratio of 1.19 +/− 0.19 (Students' 2-tailed T-test p-value: 1.06×10^{-8}). Figure 7(C and D) shows cells representative of the population average. A montage of these cell images is presented in Figure S4.

DGKδ1-Mediated Inhibition of CopII-Coated Vesicle Formation

DGKδ1 has been shown to localize to the surface of the ER (11) and it seems reasonable to speculate that a sheet structure could be appropriate for localization or activity at membrane surfaces. Overexpression of DGKδ1 can inhibit anterograde ER to Golgi transport and has been shown to specifically prevent the formation of CopII coated vesicles. This function requires both the PH and SAM domains. In order to assess whether zinc binding is involved in ER to Golgi transport regulation, we transiently transfected a number of GFP-DGKδ1 constructs into a Cos7 cell line stably expressing Sec13-YFP, a marker that localizes to CopII coated vesicles. (Fig. 8) As demonstrated previously, overexpression of GFP-DGKδ1-WT prevents formation CopII coated vesicles, visualized as a loss of YFP puncta in cells expressing the GFP-wild type DGK fusion while Sec13-YFP puncta are still clearly visible in large numbers in surrounding cells without a GFP signal. (Fig. 8A) Deletion of the SAM domain neutralizes this effect (Fig. 8B). The introduction of mutations that block polymerization (V52E) or eliminate zinc binding (DGKδSAM^{ZnMut}) into the DGKδ1 construct achieves an effect similar to complete deletion of the SAM domain. (Fig. 8C and 8D) These results suggest that regulation of CopII coated vesicle formation requires a fully functional SAM domain, one with both the ability to polymerize and bind zinc.

DISCUSSION

The DGKδSAM domain was previously shown to inhibit activity at the plasma membrane by retaining the protein in a cytoplasmic, vesicular localization through its ability to form helical SAM polymers (17). In this study we demonstrate that DGKδSAM binds zinc with at least two binding sites: One near the polymer interface and one on the surface of the polymer, which appears to drive the side-by-side association of the polymers into sheets. Zinc organization and stabilization of DGKδ into two-dimensional sheets may provide an additional level of regulation by helping to maintain an off state of the enzyme, consistent

with our finding that disabling zinc binding results in a subtle but significant increase in TPA-stimulated relocalization sensitivity. Zinc has long been known to stabilize the storage form of insulin and may play a similar role in the regulation of DGKδ (26). We cannot entirely exclude, however, the possibility that the mutations that inhibit zinc binding have other effects.

Two-dimensional sheets are an appropriate structure to associate with membrane surfaces. While previous work has shown that the DGKδ1 population that translocates to the plasma membrane in response to TPA stimulation is mostly monomeric (8), it is possible that the oligomeric form of DGKδ is utilized at other membrane surfaces. Consistent with this idea, we find that mutations that block polymerization or zinc binding eliminate ER localization and DGKδ1's role in antereograde ER to Golgi transport (11). Low affinity interactions with lipids or other proteins could be supplemented by the additive effect of polyvalency. Thus, the fact that DGKδ1^{ZnMut} has lost its ability to form large cytoplasmic puncta may also be the result of the lost avidity for cytoplasmic vesicles.

DGKδ splice variants display overlapping but unique expression profiles across various cell types including high levels in skeletal muscle and testes (4). The zinc content of testes is known to be significantly higher than in other tissues (24). It is possible that this difference in zinc availability might offer the opportunity for DGKδ to fine-tune its behavior in different cell types. In this case, a zinc-induced shift of oligomeric state could serve as a means of further adapting DGKδ behavior to a specific cell type without the need for additional tissue-specific splice variants.

Our results show that both Shank3SAM and DKGδSAM form zinc-dependent sheets, which suggests that other SAM domains may possess similar capabilities. The fact that the zinc binding sites are not conserved, however, makes predictions difficult. Nevertheless, zinc binding and sheet formation must be considered as possible roles for other SAM domains.

Supplementary Material

Refer to Web version on PubMed Central for supplementary material.

Acknowledgments

The authors would like to thank Dr. Matthew Schibler and Dr. Martin Phillips for technical support with confocal microscopy and SPR equipment, respectively. The Cos7 cell line stably expressing Sec13-YFP was generously provided by Dr. Ikuo Wada and the mCherry-Clathrin construct by Dr. Klemens Rottner. We would also like to thank Tracy M. Blois, Ryan L. Stafford, and Tyler P. Korman for manuscript review and Hao Li for stock solution preparation.

This work was supported by NIH grant R01GM093393 and R01CA081000 to JUB.

ABBREVIATIONS

TPA	12-O-tetradecanoylphorbol-13-acetate
DG	Diacylglycerol
DGK	Diacylglycerol Kinase
EM	electron microscopy
EH	End-Helix
ER	endoplasmic reticulum

ICP-MS	inductively coupled mass spectrometry
MBP	maltose binding protein
ML	Mid-Loop
PA	phosphatidic acid
PH	plekstrin homology
SAM	Sterile Alpha Motif

References

1. Nishizuka Y. Intracellular signaling by hydrolysis of phospholipids and activation of protein kinase C. Science. 2001; 258:607–614. [PubMed: 1411571]
2. Luo B, Regier DS, Prescott SM, Topham MK. Diacylglycerol kinases. Cell Signal. 2004; 16:983–989. [PubMed: 15212759]
3. Sakane F, Imai S, Kai M, Yasuda S, Kanoh H. Diacylglycerol kinases: why so many of them? Biochim Biophys Acta. 2007; 1771:793–806. [PubMed: 17512245]
4. Sakane F, Imai S, Kai M, Wada I, Kanoh H. Molecular cloning of a novel diacylglycerol kinase isozyme with a pleckstrin homology domain and a C-terminal tail similar to those of the EPH family of protein-tyrosine kinases. J Biol Chem. 1996; 271:8394–8401. [PubMed: 8626538]
5. Klauck TM, Xu X, Mousseau B, Jaken S. Cloning and Characterization of a Glucocorticoid-induced Diacylglycerol Kinase. J Biol Chem. 1996; 271:19781–19788. [PubMed: 8702685]
6. Imai S, Kai M, Yasuda S, Kanoh H, Sakane F. Identification and Characterization of a Novel Human Type II Diacylglycerol Kinase, DGKκ. J Biol Chem. 2005; 280:39870–39881. [PubMed: 16210324]
7. Murakami T, Sakane F, Imai S, Houkin K, Kanoh H. Identification and characterization of two splice variants of human diacylglycerol kinase eta. J Biol Chem. 2003; 278:34364–34372. [PubMed: 12810723]
8. Imai S, Sakane F, Kanoh H. Phorbol ester-regulated oligomerization of diacylglycerol kinase delta linked to its phosphorylation and translocation. J Biol Chem. 2002; 277:35323–35332. [PubMed: 12084710]
9. Sakane F, et al. Alternative splicing of the human diacylglycerol kinase delta gene generates two isoforms differing in their expression patterns and in regulatory functions. J Biol Chem. 2002; 277:43519–43526. [PubMed: 12200442]
10. Kawasaki T, Kobayashi T, Ueyama T, Shirai Y, Saito N. Regulation of clathrin-dependent endocytosis by diacylglycerol kinase delta: importance of kinase activity and binding to AP2alpha. Biochem J. 2008; 409:471–479. [PubMed: 17880279]
11. Nagaya H, Wada I, Jia Y, Kanoh H. Diacylglycerol kinase delta suppresses ER-to-Golgi traffic via its SAM and PH domains. Mol Biol Cell. 2002; 13:302–316. [PubMed: 11809841]
12. Chibalin AV, et al. Downregulation of diacylglycerol kinase delta contributes to hyperglycemia-induced insulin resistance. Cell. 2008; 132:375–386. [PubMed: 18267070]
13. Kim CA, et al. Polymerization of the SAM domain of TEL in leukemogenesis and transcriptional repression. EMBO J. 2001; 20:4173–4182. [PubMed: 11483520]
14. Baron MK, et al. An architectural framework that may lie at the core of the postsynaptic density. Science. 2006; 311:531–535. [PubMed: 16439662]
15. Kim CA, Sawaya MR, Cascio D, Kim W, Bowie JU. Structural organization of a Sex-comb-on-midleg/polyhomeotic copolymer. J Biol Chem. 2005; 280:27769–27775. [PubMed: 15905166]
16. Qiao F, Bowie JU. The many faces of SAM. Sci STKE. 2005; 2005:re7. [PubMed: 15928333]
17. Harada BT, et al. Regulation of enzyme localization by polymerization: polymer formation by the SAM domain of diacylglycerol kinase delta1. Structure. 2008; 16:380–387. [PubMed: 18334213]
18. Harding MM. The geometry of metal–ligand interactions relevant to proteins. Acta Crystallogr D Biol Crystallogr. 1999; 55:1432–1443. [PubMed: 10417412]

19. Harding MM. The geometry of metal–ligand interactions relevant to proteins. II. Angles at the metal atom, additional weak metal–donor interactions. Acta Crystallogr D Biol Crystallogr. 2000; 56:857–867. [PubMed: 10930832]

20. Harding MM. Geometry of metal–ligand interactions in proteins. Acta Crystallogr D Biol Crystallogr. 2001; 57:401–411. [PubMed: 11223517]

21. Harding MM. The architecture of metal coordination groups in proteins. Acta Crystallogr D Biol Crystallogr. 2004; 60:849–859. [PubMed: 15103130]

22. Harding MM. Small revisions to predicted distances around metal sites in proteins. Acta Crystallogr D Biol Crystallogr. 2006; 62:678–682. [PubMed: 16699196]

23. Berks BC. Biochemistry: Cells enforce an ion curtain. Nature. 2008; 455:1043–1044. [PubMed: 18948937]

24. Versieck J, McCall JT. Trace Elements in Human Body Fluids and Tissues. Critical Reviews in Clinical Laboratory Sciences. 1985; 22:97–184. [PubMed: 3891229]

25. Pettit FK, Bare E, Tsai A, Bowie JU. HotPatch: A Statistical Approach to Finding Biologically Relevant Features on Protein Surfaces. J Mol Biol. 2007; 369:863–879. [PubMed: 17451744]

26. Dunn MF. Zinc–Ligand Interactions Modulate Assembly and Stability of the Insulin Hexamer – A Review. BioMetals. 2005; 18:295–303. [PubMed: 16158220]

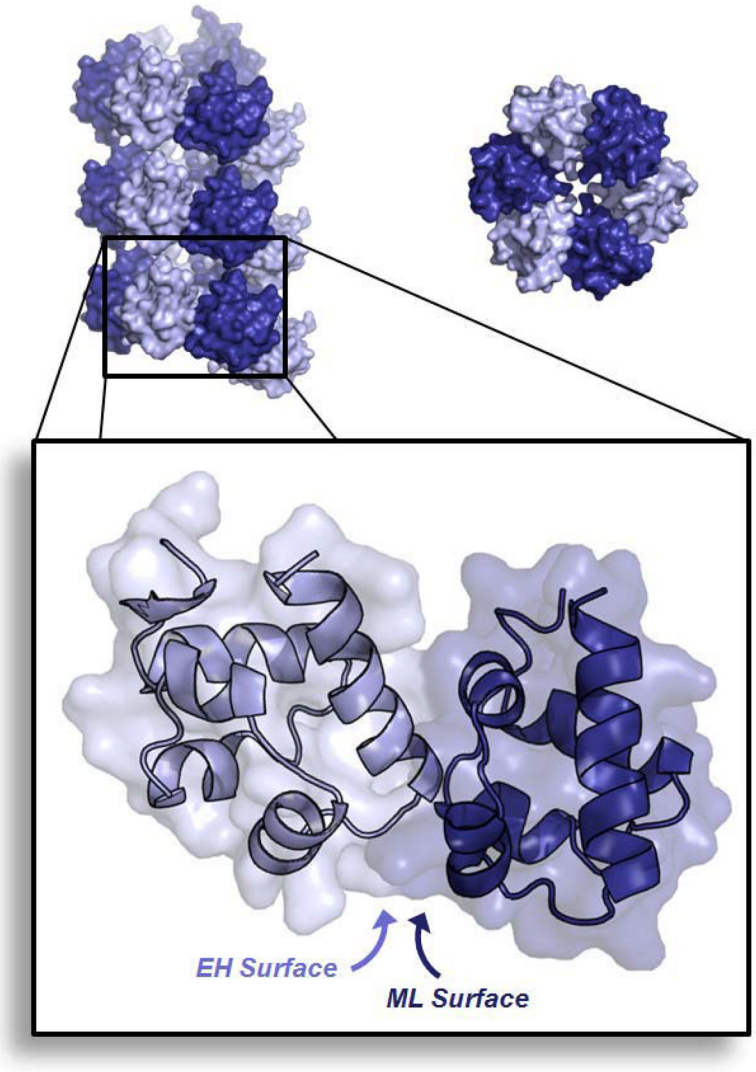

Fig. 1.
The DGKδSAM Polymer. Top left: A space-filling representation of several turns of the helical DGKδSAM polymer perpendicular to the polymer axis. Every other subunit is colored light blue or dark blue. Top right: The polymer viewed down the polymer axis. Bottom: Two subunits of the polymer shown in isolation. The EH SAM interaction surface resides on the light blue subunit and the ML surface resides on the dark blue subunit.

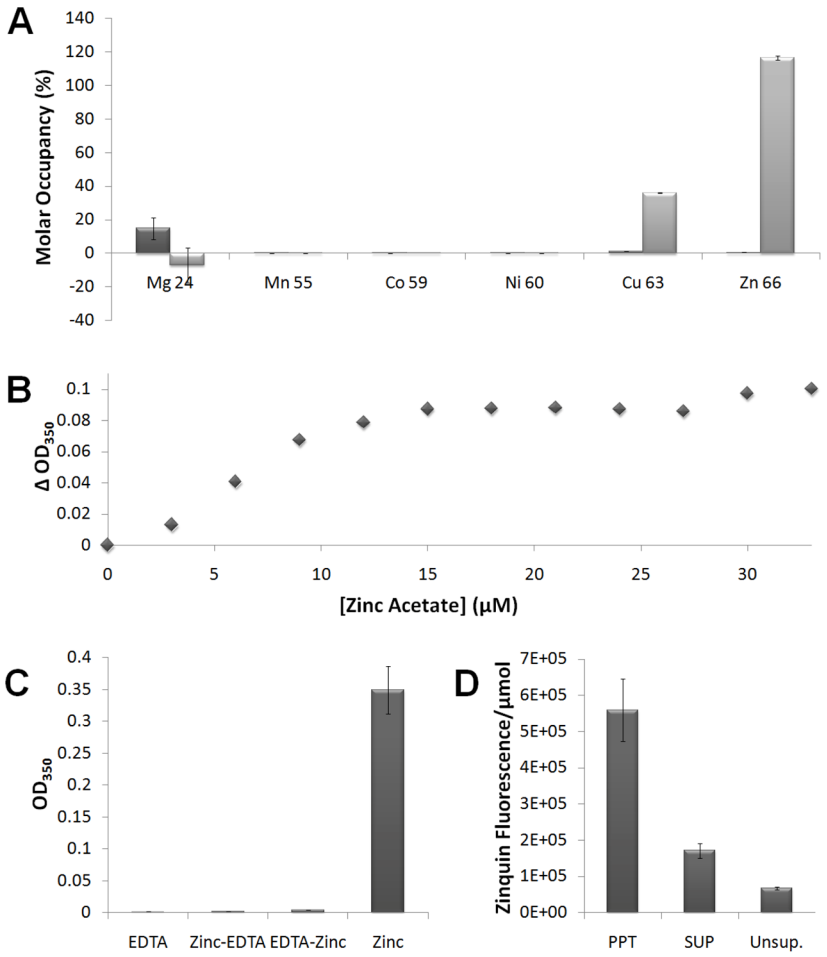

Fig. 2.

Zinc is bound by DGKδSAM and induces a shift to higher molecular weight species. (A) Metal binding by DGKδSAM. DGKδSAM-WT (light grey bars) and MBP (dark grey bars) were incubated with equal concentration of metal sulfate solutions and the total metal content was determined by ICP-MS. The molar percent occupancy of metal ions in a given protein sample is shown. (B) Zinc binding drives aggregation. The turbidity (A_{350}) of a 20 μM tag free DGKδSAM-E35G protein incubated with various concentrations of zinc acetate is shown. (C) Zinc induced aggregation is reversible. Tag-free DGKδSAM-E35G protein was either incubated with zinc, zinc followed by EDTA, EDTA followed by zinc, or just EDTA. The turbidity after 24 hours is shown. (D) Zinc is associated preferentially with insoluble material. 37 μM tag free DGKδSAM-E35G protein was incubated in buffer supplemented with 7.4 μM Zn or without additional Zn supplementation. The zinc-precipitated fraction was separated from the remaining soluble protein and all samples were denatured and zinc assayed by Zinquin fluorescence. The fluorescence per μmol protein is shown. ‘PPT’ refers to the zinc-precipitated protein fraction, ‘SUP’ to the remaining soluble supernatant, and ‘unsup’ to the protein sample incubated in zinc-free buffer.

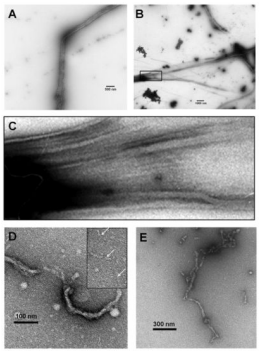

Fig. 3.

Zinc induces formation of DGKδSAM sheet oligomers. DGKδSAM protein samples were refolded in the absence or presence of zinc acetate and then visualized by electron microscopy. (A) DGKδSAM-E35G without added zinc. The protein is almost entirely monomeric, but some polymers are found (perhaps due to residual zinc) with the expected 8 nm diameter, which associate lengthwise to form ribbons. (B) DGKδSAM-E35G + 50 μM zinc. Large sheet structures are formed. (C) A close up view of the boxed portion of frame B. Sheet striations are visible suggesting that the sheets are formed by association of polymers. (D) DGKδSAM^{ZnMut} without added zinc. A rare, bundled polymer species similar to those seen previously for wild type is shown. Single, unbundled polymers from the same grid shown in inset are the dominant polymer species (arrows). (E) DGKδSAM^{ZnMut} + 1000μM zinc. Slightly longer, more prevalent polymers are apparent with added zinc, but not large sheets.

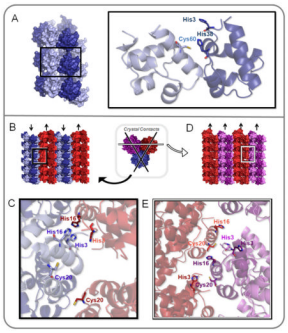

Fig. 4.

Zinc binding residues cluster at both inter- and intra-polymer interfaces. (A) Possible zinc binding residues that cluster in the intra-polymer interface. Left: A space-filling representation of several turns of the helical polymer perpendicular to the polymer axis. Right: Two subunits of the polymer shown in isolation showing Cys60 and His38 side chains. His3 is also displayed because it is on a flexible portion of the protein and could potentially participate in zinc binding. (B – E) Possible zinc binding residues that cluster between polymers. The crystal structure included both parallel and antiparallel association of polymers in its packing and either one could create sheets. (B) The antiparallel association of helical polymers. (C) Possible zinc binding residues that cluster at the antiparallel interface. (D) The parallel association of polymers. (E) Possible zinc binding residues that cluster at the parallel interface.

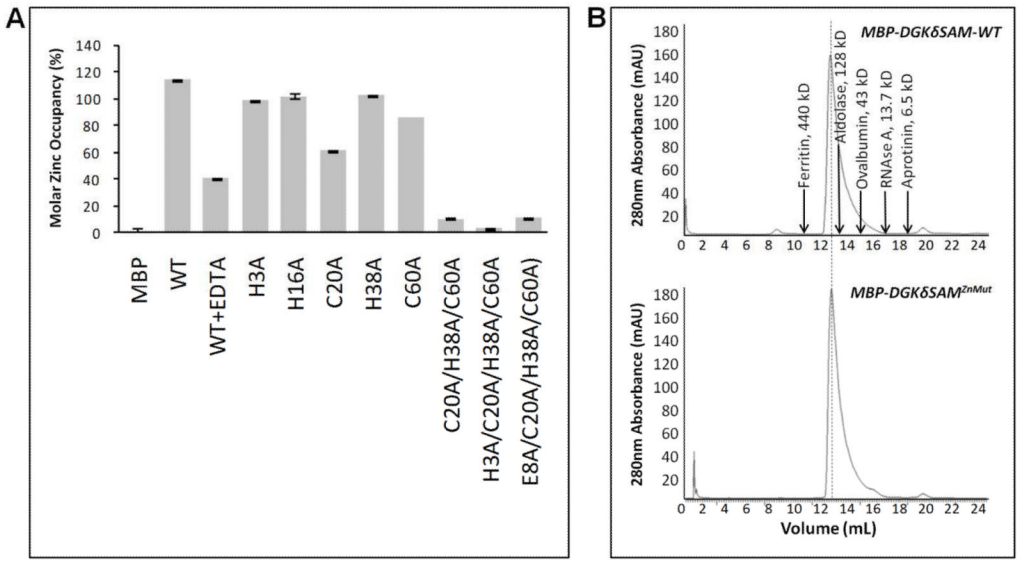

Fig. 5.

Residues involved in DGKδSAM zinc binding. (A) Zinc binding by DGKδSAM mutants. MBP-fusion constructs of DGKδSAM-WT or those containing alanine substitutions were incubated in the presence of 1mM zinc acetate and dialyzed extensively against zinc-free buffer. Samples were then analyzed by ICP-MS to measure the amount of retained metal. The percent molar zinc occupancy is shown. (B) DGKδSAM^{ZnMut} has similar self-association properties as the wild-type protein in the absence of zinc. MBP-DGKδSAM-WT and MBP-DGKδSAM^{ZnMut} samples were applied to a gel filtration column after incubation with 1mM EDTA. The two samples are virtually superimposable except for the presence of a small peak in the void volume of the wild-type profile.

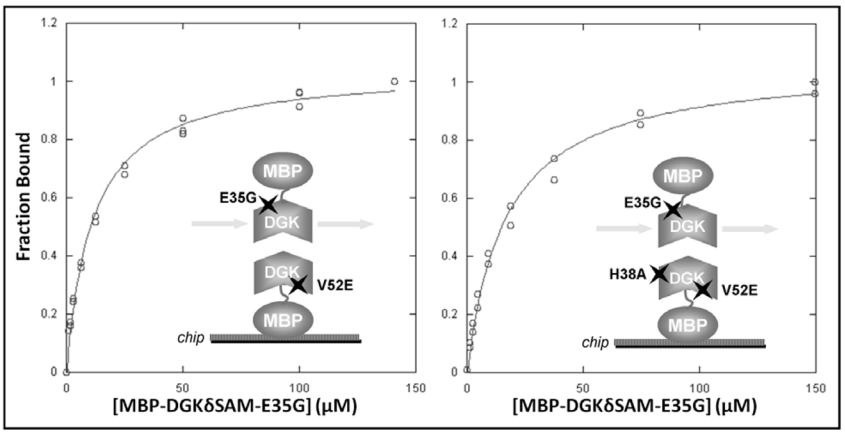

Fig. 6.

H38A, a zinc binding substitution in the intra-polymer interface does not significantly impact polymer association in the absence of zinc. To measure the affinity between subunits in the polymer, without complications from polymerization, we measured binding between a mutant (V52E) that blocks the EL surface and a mutant (E35G) that blocks the ML surface. This leaves an intact ML surface on the V52E mutant and an intact EH surface on the E35G mutant for binding. Here, either MBP-DGKδSAM-V52E or MBP-DGKδSAM-H38A/V52E was immobilized on an SPR chip and various concentrations of MBP-DGKδSAM-E35G were applied to the chips. The equilibrium SPR response was measured. The resulting binding curves are shown. The curves were fit to a hyperbolic binding isotherm.

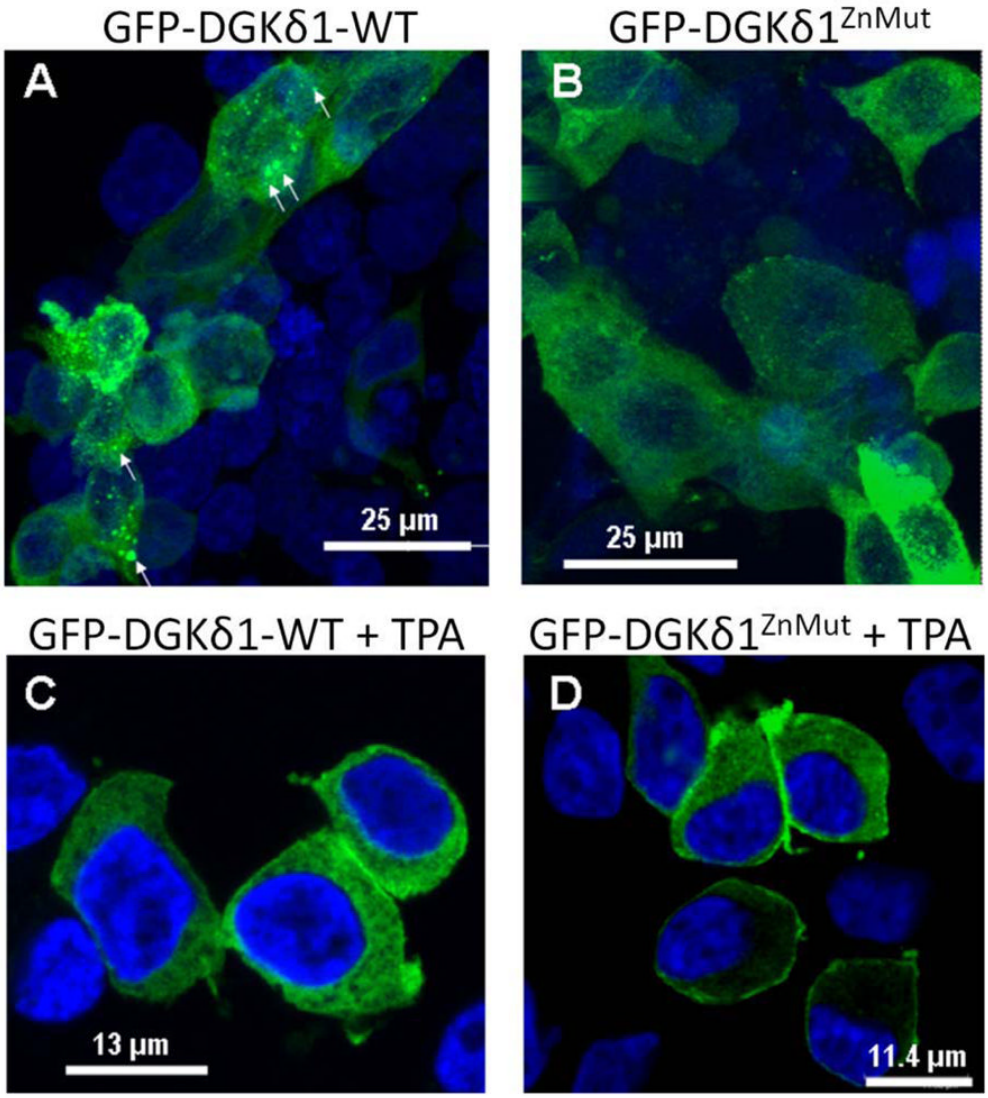

Fig. 7.

Zinc site mutations impair DGKδ1 localization to cytoplasmic puncta and enhance localization the plasma membrane. (A and B) Projections through HEK293 cells transiently transfected with GFP-DGKδ1 constructs. The GFP-DGKδ1-WT construct forms large cytoplasmic puncta (several are indicated by white arrows), which are reduced or absent when the zinc site mutations are introduced. (C and D) Single images of HEK293 cells transiently transfected with GFP-DGKδ1 constructs followed by incubation with 0.45 μM TPA. Cells transfected with the DGK construct containing the zinc site mutations show an enhanced propensity to localize to the plasma membrane. Additional images are shown in supplemental Figure S4.

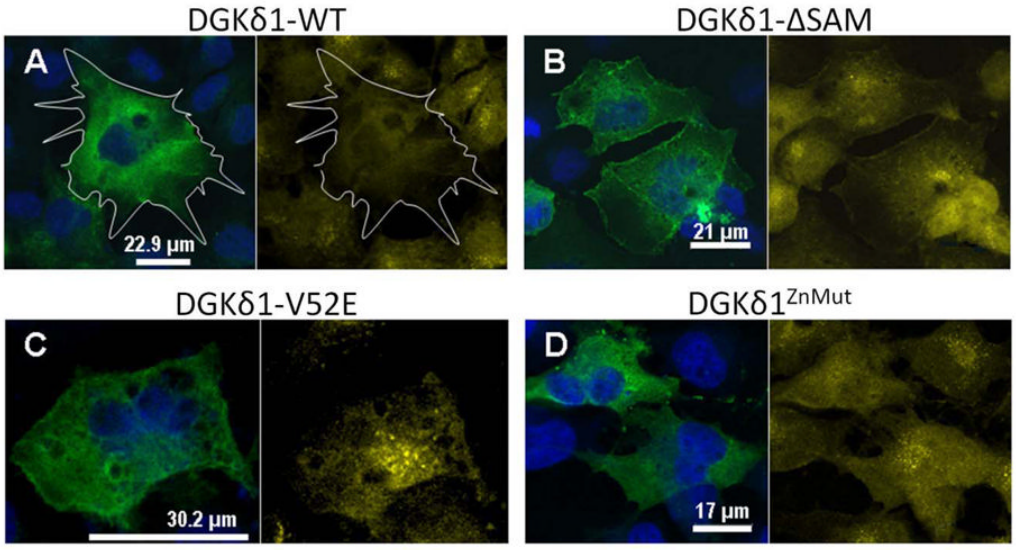

Fig. 8.

Zinc binding mutations impair DGKδ1 inhibition of CopII-coated vesicle formation. Cos7 cells stably expressing Sec13-YFP, a marker for CopII coated vesicles, were transiently transfected with GFP-DGKδ1 constructs. Each set of images shows the overlapping signals for Dapi (blue) and GFP (green) at the left and the YFP signal (yellow) at the right. Cells displaying CopII vesicle formation are peppered with small puncta. White arrows indicate a few representative examples of such puncta. (A) GFP-DGKδ1-WT expression is mutually exclusive with the formation of Sec13-YFP puncta. A cell strongly expressing the DGK construct is outlined in white and does not contain yellow puncta like its neighboring counterparts which do not express the DGK construct. (B) GFP-DGKδ1-ΔSAM-expressing cells still show the formation of Sec13-YFP puncta. (C) GFP-DGKδ1-V52E-expressing cells also show the formation of Sec13-YFP puncta. (D) GFP-DGKδ1^{ZnMut} expression also does not interfere with the normal formation of Sec13-YFP puncta.